Published in final edited form as:
J Neurosci Res. 2012 August ; 90(8): 1489–1506. doi:10.1002/jnr.23040.

PARP-1 deletion promotes subventricular zone neural stem cells toward a glial fate

Jennifer M. Plane, **Steven K. Grossenbacher**, and **Wenbin Deng**
Department of Biochemistry and Molecular Medicine, Institute for Pediatric Regenerative Medicine, School of Medicine, University of California, Davis, Sacramento, California 95817, USA

Abstract

Identification of critical factors involved in oligodendroglial fate specification from endogenous neural stem cells is relevant to the development of therapeutic interventions that aim to promote remyelination. Here we report a novel role of the DNA repair protein poly-ADP-ribose polymerase-1 (PARP-1) in regulating the neural stem cell profile in the postnatal mouse forebrain subventricular zone (SVZ). We observed increased the expression of Sox2 and Sox10 in the SVZ of postnatal day 11 (P11) PARP-1 knockout mice. This increase corresponded with increased Olig2 expression in Sox2-positive cells of the PARP-1 knockout mouse SVZ and decreased Map2abc expression, compared to Sox2/Olig2 and Sox2/Map2abc expression in wild-type mice. We noted enhanced expression of proliferating oligodendrocyte progenitor cells (OPCs) at the expense of proliferating neuroblasts in the SVZ of PARP-1 knockout mice, using Olig1/KI67/DCX, NG2/KI67/DCX and PDGFR/BrdU/TUJ1 immunofluorescence labeling. In addition, the percentage of BrdU/Olig2 double-labeled cells increased in the SVZ and corpus callosum of PARP-1 knockout mice compared to wild-type mice. We also observed a decrease in DCX-positive cells without a decrease in the overall SVZ area in PARP-1 knockout mice, further indicating a switch from neuroblast to OPC fate. PARP-1 knockout mice displayed thinning of MBP expression in the corpus callosum and external capsule, suggesting that the enhanced OPC proliferation in the SVZ might compensate for deficiency in myelination. Together, our results show that PARP-1 deletion promotes SVZ neural stem cells toward a glial fate, and suggest that future studies target PARP-1 as a potential therapeutic strategy for demyelinating diseases.

Keywords

subventricular zone; poly-ADP-ribose polymerase; oligodendrocyte progenitor cells

Introduction

Neural stem cells persist in the forebrain subventricular zone (SVZ), producing olfactory bulb interneurons in the adult rodent whereas they produce neurons, astrocytes and oligodendrocytes during development (Altman, 1969; Corotto et al., 1993; Kaplan and Hinds, 1977; Lois and Alvarez-Buylla, 1993, 1994). The SVZ contains three types of neural stem cells, identified as type A, B and C cells (Doetsch et al., 1997). These cells are identified based on their protein and transcription factor expression. Type B cells, the putative neural stem cells, express glial fibrillary acidic protein (GFAP) and asymmetrically divide to produce type B and C cells (Doetsch et al., 1997). Type C cells, transit-amplifying

Corresponding Author: Dr. Wenbin Deng, Associate Professor Department of Biochemistry and Molecular Medicine University of California, Davis 2425 Stockton Blvd., Room 653 Sacramento, CA, 95817 wbdeng@ucdavis.edu.

The authors declare no conflicts of interest.

progenitors, express DLX2 and give rise to type A cells (Doetsch et al., 1997). Type A cells, neuroblasts, express doublecortin, migrate from the SVZ through the rostral migratory stream and into the olfactory bulb where they mature into interneurons (Doetsch et al., 1997; Lois and Alvarez-Buylla, 1994).

Poly (ADP-ribose) polymerase-1 (PARP-1) is one of 18 PARPs that regulate multiple cellular processes by adding poly (ADP-ribose) polymers to specific proteins (Ame et al., 2004; Chambon et al., 1963; Kim et al., 2005). PARP-1 is the most abundantly expressed (Moroni, 2008; Sodhi et al.) and was initially identified as the DNA single-strand break repair enzyme (Fernet et al., 2000; Masson et al., 1998; Tartier et al., 2003). PARP-1 modulates transcription, directly affecting gene expression by localizing to the promoters of actively transcribed genes (Hassa and Hottiger, 2002; Kraus and Lis, 2003; Krishnakumar et al., 2008). PARP-1 regulates chromatin structure, functions as a co-regulator (Krishnakumar and Kraus), functions in DNA replication (Sugimura et al., 2008), epigenetics (Krishnakumar et al., 2008; Quenet et al., 2009), and memory consolidation (Fontan-Lozano et al.; Goldberg et al., 2009; Hernandez et al., 2009). PARP-1 over-activation leads to cellular energy store depletion, cell dysfunction and death (Meyer-Ficca et al., 2005), and is strongly implicated in the pathogenesis of stroke, myocardial infarction, and inflammatory and neurodegenerative disorders. As PARP-1 functions in numerous cellular processes including DNA repair, cell death, transcription co-activation, and chromatin plasticity, we examined the hypothesis that PARP-1 regulates neural stem cell fate in the postnatal mouse forebrain SVZ.

Few studies have examined the role of PARP-1 in stem cells. Embryonic stem cell (ESC) gene analysis of PARP-1 KO mice revealed a significant shift in “stemness” genes, suggesting that PARP-1 modulates ESC gene activity (Ogino et al., 2007). PARP-1 also poly(ADP-ribosyl)ates an important pluripotency gene, Sox2, in ESCs (Gao et al., 2009). PARP-1 inhibition increased Sox2 protein and compromised cell growth and survival during differentiation. Another study revealed a requirement for PARP-1 in the cofactor exchange regulated by HES1 in neural stem cells (Ju et al., 2004). In addition, PARP-1 has been implicated in promoting differentiation of regulatory T cells and parietal endoderm-like cells (Nasta et al.; Quenet et al., 2009). Together, these studies suggest that PARP-1 plays a role in stem cell maintenance and differentiation.

No studies to date have examined the effects of PARP-1 on postnatal neural stem cells. Here, we examined the postnatal forebrain SVZ neural stem cells of PARP-1 KO mice. Our results unexpectedly demonstrate that PARP-1 depletion promotes SVZ neural stem cells toward a glial, rather than neuronal fate.

Materials and Methods

Animal protocols

Breeding pairs with a homozygous deletion of the PARP-1 gene (KO; 129S Parp1 tm1Zqw/J) and wild-type (WT) controls from the same 129S genetic background (129S1/SvlmJ) were purchased from Jackson Laboratories (Bar Harbor, ME). Mice were bred and genotyped and offspring were used at postnatal day eleven (P11; n=8–9/genotype/gender) for all studies. Animals were maintained in accordance with the National Institute of Health's Guide for the Care and Use of Laboratory Animals; all protocols were approved by the Institutional Animal Care and Use Committee of the University of California, Davis.

Body and brain weight measurements

Select litters were used solely to analyze brain and body weight at P11. Mice of each genotype were weighed and sexed (n=9–10 animals/group). Mice were anesthetized with

CO_2 and decapitated. Brains were removed and wet brain weight obtained for the whole brain, which included olfactory bulbs, forebrain, midbrain, hindbrain and cerebellum. To ensure consistency, all weights were obtained using the same scale.

BrdU labeling

The thymidine analog, 5-Bromo-2'-deoxyuridine (BrdU, Roche, Indianapolis, IN) was used to label cells in S-phase (Miller and Nowakowski, 1988). Mice received intraperitoneal (i.p.) injections of BrdU (100 mg/kg in sterile PBS) two hours prior to sacrifice.

Histology

Animals were deeply anesthetized (ketamine 100 mg/kg and xylazine 10 mg/kg, i.p.) and transcardially perfused with saline and 4% paraformaldehyde (PFA). Brains were removed and post-fixed in 4% PFA overnight, cryoprotected in 20% sucrose, then embedded in a 2:1 20% sucrose/OCT embedding medium (Sakura Finetek, Torrence, CA) and frozen on powdered dry ice. Coronal serial sections were cut at 30 μm on a cryostat and free-floating sections were collected and stored in 0.1 M Tris in 12-well plates (stored at 4°C) for immunohistochemistry and immunofluorescence. Sections were transferred to cryoprotectant and stored at −20°C for long-term storage. To assess SVZ and hemisphere size, sections were slide-mounted and Nissl-stained using cresyl violet. A computerized video camera-based image analysis system (with ImageJ v.1.43 software) was used to measure bilateral regional cross-sectional SVZ area and density as well as hemisphere area on four coronal sections per brain at levels encompassing the entire striatum and SVZ as described previously (Plane et al., 2004).

Immunohistochemistry

Diaminobenzidine (DAB) immunohistochemistry was performed on every 12th section with antibodies to doublecortin (DCX; 1:2000; anti-goat, Santa Cruz Biotechnology, Santa Cruz, CA) or myelin basic protein (MBP; 1:1000; anti-mouse, Covance, Berkeley, CA) following previously published protocols (Plane et al., 2008). Sections were rinsed in Tris (0.1 M, pH 7.6), blocked with 10% normal horse serum, and incubated overnight at 4°C with anti-DCX or anti-MBP. Sections were rinsed, incubated in secondary antibody (1:200 biotinylated horse anti-mouse IgG or horse anti-goat IgG, Vector Labs, Burlingame, CA) for 1 h, rinsed, signal amplified with Vector ABC kit, developed with stable DAB (Invitrogen, Carlsbad, CA), mounted onto slides, dehydrated and cleared in ethanol and xylenes, and coverslipped using Permount (Sigma, St. Louis, MO).

Double DAB staining was performed with antibodies to BrdU (1:1000; anti-mouse, Roche Applied Science, Indianapolis, IN) and CD133 (prominin-1; 1:1000; anti-rat, Millipore). Sections were washed in tris, denatured in 2N HCl at 37°C for 30 min, neutralized in 0.1 M boric acid for 10 min, rinsed, blocked with 10% normal horse serum (Invitrogen), and incubated overnight at 4°C with anti-BrdU antibody. Sections were rinsed, incubated in secondary antibody (1:200 biotinylated horse anti-mouse IgG, Vector Labs) for 1 h, rinsed, signal amplified with Vector ABC kit, and developed with Vector VIP kit. Sections were washed and blocked with 10% normal rabbit serum (Vector labs), and incubated overnight at 4°C with anti-CD133. Sections were washed, incubated in biotinylated rabbit anti-rat IgG (1:200, Vector Labs), signal amplified with Vector ABC kit, and developed with stable DAB (Invitrogen). Sections were mounted onto slides, dehydrated and cleared in ethanol and xylenes, and coverslipped using Permount (Sigma).

For non-BrdU double or triple label immunofluorescence staining, sections were washed with Tris-Buffered Saline (TBS), blocked in goat or donkey serum, then incubated in primary antibodies overnight at 4°C (anti-rabbit Sox2, 1:1000, Millipore; anti-goat Olig2,

1:200, R&D Systems, Minneapolis, MN; anti-mouse Olig1, 1:200, Millipore; anti-mouse NG2, 1:100, Millipore; anti-mouse PARP-1, 1:100, Trevigen, Gaithersburg, MD; anti-mouse Map2abc, 1:500, Sigma; anti-rabbit Ki67, 1:2000, Vector Labs; anti-goat Sox10, 1:200, Millipore; anti-mouse O4, 1:200, Millipore). Sections were washed in TBS, blocked briefly, and then incubated in the appropriate species- and isotype-specific Alexa 488, 594 or 647 secondary antibodies (1:800, Invitrogen) for 1.5 hours. Sections were washed, counterstained with 4,6-diamidino-2-phenylindole (DAPI, 1 μM final concentration; Invitrogen) for 5 min, mounted onto slides and allowed to dry, then coverslipped with an anti-fade medium (Pro-Long, Invitrogen).

To identify dividing SVZ oligodendrocyte progenitor cells or neuroblasts, sections were double or triple-labeled with antibodies to BrdU (1:250; anti-rat, Accurate Chemicals, Westbury, NY), TUJ1 (1:500; anti-mouse, Covance), Olig2 (1:500; anti-rabbit, Millipore) or PDGFR-α (1:200; anti-rabbit, Santa Cruz Biotechnology). Sections were washed in TBS, denatured in 2N HCl at 37°C for 30 min, neutralized in 0.1 M boric acid for 10 min, rinsed, blocked with goat serum and then incubated in both primary antibodies overnight at 4°C. Sections were washed in TBS, blocked briefly, and then incubated in goat-anti-rat Alexa 594 and goat-anti-rabbit Alexa 488 (Invitrogen) for 1.5 hours. Sections were washed, mounted onto slides and allowed to dry, then coverslipped with an anti-fade medium (Pro-Long, Invitrogen).

RNA isolation and qPCR

We used quantitative polymerase chain reaction (qPCR) to examine the relative expression of PARP-1 (Mm00500171_g1), Sox2 (Mm00488369_s1), Sox10 (Mm00569909_m1), and Olig2 (Mm01210556_m1) in the SVZ of PARP-1 KO and wild-type mice. P11 mice were deeply anesthetized (100 mg/kg ketamine and 10 mg/kg xylazine, i.p.) and then perfused with 0.1 M PBS. Brains were removed and the SVZ and cortex dissected out and flash frozen in liquid nitrogen. Samples were stored in liquid nitrogen until the time of use. RNA was isolated using the Qiagen RNeasy lipid mini kit following the standard protocol (Qiagen, Valencia, CA). RNA purification was verified using the OD 260/280 ratio. Total RNA (1.0 μg) was reverse-transcribed to cDNA using TaqMan® Reverse Transcription Reagents (Applied Biosystems, Foster City, CA). Glyceraldehyde-3-phosphate dehydrogenase (GAPDH; Beacon Designer) was used as the housekeeping gene. qPCR reactions were performed in triplicate on a Roche Lightcycler 480 using the TaqMan primers listed above. Validation was performed by calculating qPCR efficiencies by the amplification of a standardized dilution series, and constructing a relative efficiency plot comparing target and reference ΔCp values to ensure that the absolute slope of fit line was less than 0.1. Subsequently, all experimental samples were analyzed and normalized with the expression level of the internal control gene, GAPDH. Relative quantification of fold-change was performed by applying the $2^{-\Delta\Delta}Ct$ method and comparing Cp values (calculated by second derivative maximum) of SVZ tissue to cortical tissue (control) for PARP-1 KO and wild-type mice (Livak and Schmittgen, 2001).

Cell counting and unbiased stereology

All quantitative analyses were performed without the knowledge of experimental condition to avoid biases. Unbiased stereology was performed on every 12th section (n=4 sections/mouse) to count BrdU-positive or Sox2-positive cells in the SVZ. SVZ areas were outlined at low magnification and BrdU-positive or Sox2-positive cells were counted at 100× using the optical fractionator technique (Plane et al., 2004; West et al., 1996). Images of the dorsolateral SVZ were captured using an Olympus BX61-DSU microscope (Olympus Corp., Melville, NY) and Hamamatsu ORCA-ER camera (Hamamatsu Photonics, Shizuoka, Japan) at 60× magnification to quantify Ki67-positive cells. Images were imported into Adobe

Photoshop CS2, Ki67-positive cells counted in 4 equidistant SVZ static images per mouse, and data entered into Microsoft Excel for graphic analysis. Images of the SVZ were captured using the same aforementioned Olympus microscope and camera at 10× magnification for DCX- and MBP-stained sections. DCX immunoreactivity was quantified in the SVZ in 4 equidistant anterior striatal sections per animal. DCX-positive SVZ area measurements were obtained using Image J from 10× images of the dorsolateral SVZ. For CD133 analysis, 100× images of the lateral ventricle/dorsolateral SVZ were captured using the same Olympus microscope and Hamamatsu camera. Cells were counted in 4 static images per mouse using Adobe Photoshop CS2. For BrdU/Olig2 double-label analysis, a Nikon Eclipse C1 confocal laser scanning microscope with 40× objective was used to image Alexa 488 (green) or Alexa 594 (red). Z-series stacks (1 μm thick optical slices) were collected from 4 equidistant SVZ sections and viewed using the Nikon EZ-C1 3.20 Free Viewer software, version 3.8 for the SVZ and corpus callosum. This software was used to create single-channel and merged views for double-labeling to quantify BrdU+ or BrdU+/Olig2+ cells, and then images were imported into Adobe Photoshop to combine and label images. For all fate change analyses, including Sox2/Map2abc/Olig2, KI67/DCX/Olig1, KI67/DCX/NG2, and BrdU/TUJ1/PDGFR-α staining, images were collected using a Nikon A1 confocal laser scanning microscope with Nikon NIS-Elements AR 3.10 software. We visualized all 4 channels (aforementioned plus DAPI) in the same field of the dorsolateral tail of the SVZ using a 60× objective in 4 sections per animal and analyzed z-stacks to determine if co-localization occurred. Sox2-positive cells were assessed for co-localization with the neuroblast maker, Map2abc, or the oligodendrocyte progenitor cell (OPC) marker, Olig2 while KI67-positive cells were assessed for co-localization with the neuroblast marker, DCX, or the OPC markers, Olig1 or NG2. In addition, BrdU-positive cells were assessed for co-localization with the neuroblast marker, TUJ1, or the OPC marker, PDGFR-α. Images were imported into Adobe Photoshop for final labeling. Images of the corpus callosum overlying the SVZ were also obtained using the Nikon A1 laser confocal microscope and Nikon NIS-Elements software. The same multi-label analyses were performed on corpus callosum images as were performed on SVZ images to determine the fate of Sox2, BrdU or KI67 cells. In addition, 4 SVZ sections per animal were analyzed for Olig2/Sox2/PARP-1 co-expression using a 100× objective on the same Nikon A1 laser confocal microscope and Nikon NIS-Elements software.

Statistics

Analysis of variance (ANOVA) with Tukey *post hoc* tests were used to compare differences between groups for all quantitative analyses. Results are presented as mean ± standard error of the mean (SEM) unless otherwise noted. Data were considered statistically significant when $p \leq 0.05$.

Results

As the PARP-1 pathway is a multi-faceted and multi-functional pathway that can be activated by a variety of circumstances, here we examined whether PARP-1 deficiency would alter the profile of SVZ neural stem cells in the postnatal forebrain. We specifically examined P11 mice for these studies to determine how PARP-1 depletion affects oligodendrogliogenesis, which peaks during the postnatal period. We thoroughly examined the SVZ cell population in both male and female P11 PARP-1 KO mice and compared them with WT on the same S129 genetic background.

PARP-1 deletion enhances Sox2-positive SVZ cells directed toward an oligodendroglial fate

A recent report from Gao et al (2009) revealed a novel role for PARP-1 in regulating embryonic stem cell properties. They discovered that PARP-1 acted as a cofactor of Oct4 and Sox2, transcription factors that regulate stem cell state, to regulate fibroblast growth factor-4 (FGF4) expression in embryonic stem cells (Gao et al., 2009). They found increased Sox2 protein expression when PARP-1 activity was inhibited or absent and determined that PARP-1 interacts with and poly(ADP-ribosyl)ates Sox2 directly. Thus, we examined whether Sox2 protein expression was altered in the SVZ of PARP-1 KO mice. We performed immunofluorescence labeling with an antibody to Sox2 and used unbiased stereology to obtain a population estimate for the SVZ. We observed more Sox2-positive cells in the SVZ of PARP-1 KO mice (Figure 1B) than in WT mice (Figure 1A). When we performed cell quantification using stereology, we found that almost twice as many Sox2-positive cells were present in the SVZ of PARP-1 KO mice (217,291 ± 11,951 cells/SVZ) compared to WT mice (130,069 ± 8,835 cells/SVZ), indicating a significant enhancement of the Sox2-positive SVZ cell population in PARP-1 KO mice (Figure 1C, $p<0.01$) compared to WT mice. Thus, PARP-1 deficiency enhances the Sox2-positive SVZ neural stem cell population.

Gao et al (2009) reported effects on embryonic stem cell growth and survival when PARP-1 was inhibited and found these effects to be specific to the differentiation state. The second postnatal week is a time of ongoing neurogenesis and oligodendrogliogenesis and alterations in the neural stem cell population during this time of elevated cell genesis and differentiation could potentially alter cell fate. Thus, we hypothesized that Sox2 upregulation in PARP-1 KO mice could be associated with upregulation of a specific progenitor population. We performed triple-label immunofluorescence for Sox2, Olig2 and Map2abc to determine if Sox2-positive cells acquired an early predisposition towards a neuronal or oligodendroglial fate and whether this was altered in PARP-1 KO mice. We used confocal microscopy to capture all 4 channels (Sox2, Olig2, Map2abc, DAPI) in the same field of the SVZ and analyzed z-stacks to determine if Sox2-positive cells expressed the OPC marker Olig2 or the neuroblast marker Map2abc. Map2abc, the neuroblast marker not to be confused with Map2ab which labels mature neurons, was chosen over DCX based on the species needed to perform this multi-labeling scheme. We found numerous Sox2-positive cells present in the SVZ of the PARP-1 KO and WT mice and again noted the increased presence of these cells in the KO mice. Numerous Olig2-positive cells were present in the SVZ and corpus callosum of all mice; however we focused on the SVZ for these analyses. The SVZ of PARP-1 KO mice contained numerous Sox2/Olig2 double labeled cells (Figure 1E, arrows) and appeared to contain more than in WT mice (Figure 1D, arrows). Of note, many of the double labeled cells appeared in the dorsal side of the SVZ, nearest to the corpus callosum. Interestingly, we found nearly three times as many Sox2/Olig2 double-labeled cells in the SVZ of PARP-1 KO mice (14.2 ± 1.8 cells/section) as were present in the SVZ of WT mice (4.9 ± 0.8 cells/section; Figure 1F, $p<0.01$). Next, we examined the expression pattern of Map2abc cells in relation to Sox2 expression. Interestingly, we observed that the pattern of Map2abc expression was not evenly distributed throughout the SVZ, but often appeared most concentrated closer to the ventricle in the dorsolateral tail, as well as at the most lateral tip of the dorsolateral tail (Figure 1G–H). Quite often this did not correspond with the most concentrated areas of Sox2 expression, which usually appeared strongest in the middle of the dorsolateral tail of the SVZ (Figure 1G–H). We also noted that cells with strong Sox2 expression often did not co-label with Olig2 or Map2abc, while those with weaker Sox2 labeling tended to co-label with Map2abc (Figure 1G). We counted the Map2abc/Sox2 double-positive cells present in the SVZ and found a significant decrease in their presence in the SVZ of PARP-1 KO mice (Figure 1H–I) compared with WT mice (Figure 1G, I,

p<0.01). Approximately twice as many Sox2/Map2abc co-labeled cells were present in WT mice (13.2 ± 1.0 cells/section) as were present in the SVZ of PARP-1 KO mice (6.9 ± 1.0 cells/section). Together, these data indicate that PARP-1 KO mice show upregulation of SVZ neural progenitor cells with an oligodendroglial fate.

PARP-1 depletion enhances SVZ cell proliferation

Many cells in the adult SVZ are quiescent and only actively proliferate upon stimulation. In the postnatal rodent brain, SVZ cell proliferation is more abundant as the brain continues to develop. We observed increased oligodendrocyte progenitor-specific proliferation and next sought to determine whether overall SVZ cell proliferation was altered in PARP-1 KO mice. First, we examined KI67 expression, an endogenous cell proliferation marker, by performing immunofluorescence labeling with an antibody to KI67. Surprisingly, more KI67-positive cells were apparent in the SVZ of PARP-1 KO mice (Figure 2B) than in wild-type mice (Figure 2A). To confirm this finding, we counted the number of KI67-positive cells in the dorsolateral tail of the SVZ. We found a significant increase in the number of KI67-positive cells in the SVZ of PARP-1 KO mice compared to WT mice (Figure 2C, p<0.01). To further confirm these findings, we next examined whether similar changes occurred in the BrdU cell population. To assess the effects of PARP-1 deficiency on SVZ cell proliferation, mice were injected with BrdU (100 mg/kg, i.p.) 2 hours prior to sacrifice. This injection time was chosen in order to get a snapshot of postnatal proliferation and based on previously published studies (Plane et al., 2004). Immunohistochemistry was performed with an antibody to BrdU to identify those cells which incorporated BrdU during the time of injection and unbiased stereology was performed to obtain a population estimate for the entire dorsolateral SVZ. BrdU immunohistochemistry revealed an apparent increase in this cell population in the SVZ of PARP-1 KO mice (Figure 2E) compared to WTs (Figure 2D), similar to that seen with KI67. Stereology further confirmed these findings and revealed that the SVZ of PARP-1 KO mice contained almost twice as many BrdU-positive cells as WT mice (Figure 2F, p<0.01). Thus, these data indicate that the SVZ of PARP-1 KO mice contains more actively dividing cells than that of the WT mice.

Recent studies suggested that the ependymal cells found along the lateral ventricle wall may also act as neural stem cells, and these cells can be identified by their expression of CD-133, also known as prominin-1 (Carlen et al., 2009; Coskun et al., 2008). Due to the increased presence of BrdU- and KI67-positive cells within the SVZ, we also examined whether this population of neural stem cells might be altered in PARP-1 KO mice. We performed immunohistochemistry with antibodies to CD-133 and BrdU and then performed cell counting on 100× images of the lateral ventricle wall at the level of the dorsolateral SVZ. CD-133-positive cells were not easily identifiable at low magnification and rarely identified along the lateral wall of the lateral ventricle in all mice. In general, most of these cells tended to be present along the dorsal and medial walls of the lateral ventricle, rather than along the lateral wall and were identifiable by their dark nucleus and long cilia extending into the ventricular space. Despite their minimal presence, we limited our quantification to the lateral wall of the ventricle, nearest the dorsolateral SVZ since this region is our area of interest for all other quantification. CD-133-positive cells were rarely present in this area in WT mice (Figure 2G). Many more CD-133-positive cells were identified in PARP-1 KO mice (Figure 2H) than WT mice, although the actual number of these cells varied highly from mouse to mouse. Quantification revealed a significant increase in CD-133-positive cells in KO mice compared to WT mice (Figure 2I, p<0.05). Of note, these cells appeared mostly in the posterior striatal sections and were not identifiable in every animal. Together, these data indicate that PARP-1 deletion enhances postnatal neural stem cell proliferation both in the SVZ and the ependymal layer.

PARP-1 deletion promotes oligodendrocyte progenitor production at the expense of neuroblast production in the SVZ

The SVZ gives rise to oligodendrocytes during the early postnatal period; however it is not clear at exactly what age the SVZ cells become primarily neurogenic. During the first two weeks of life, oligodendrocyte production and maturation peak in the mouse forebrain. Our results showing an increased presence of Sox2/Olig2 double-labeled cells in the SVZ of PARP-1 KO mice suggest that the oligodendrocyte progenitor cell (OPC) population is enhanced, likely at the expense of neurogenesis. Thus, we examined the population of proliferating OPCs and neuroblasts in the SVZ in P11 PARP-1 KO mice to determine if this population was altered by PARP-1 deficiency. We performed triple immunofluorescence staining with antibodies for BrdU or KI67 to identify proliferating cells, Olig1, NG2, or PDGFRα to identify OPCs, and DCX or TUJ1 to identify neuroblasts. Numerous DCX-positive cells were present in the SVZ of WT (Figure 3A) and PARP-1 KO (Figure 3E) mice and many of these cells co-labeled with KI67 in both genotypes (Figure 3D, H). Olig1 was also expressed in the SVZ of both genotypes but appeared to be enhanced in PARP-1 KO mice (Figure 3G) compared to WT mice (Figure 3C). In addition, more Olig1/KI67 double-labeled cells appeared in the SVZ of PARP-1 KO mice (Figure 3H, arrows) compared with WT mice (Figure 3D, arrows). To confirm an apparent increase in OPC proliferation, we examined DCX/KI67/NG2 immunofluorescence in the SVZ. Numerous DCX-positive cells were present in the SVZ of both genotypes, although there appeared to be slightly more DCX expression in the WT mouse SVZ (Figure 3I) than in the PARP-1 KO SVZ (Figure 3M). Numerous KI67-positive cells were present in both genotypes (Figure 3J, N) and some co-labeled with DCX in both genotypes (Figure 3L, P). Interestingly, we observed more NG2 expression in the SVZ of PARP-1 KO mice (Figure 3O) than in WT mice (Figure 3K) with many of these cells co-labeling with KI67 in the PARP-1 KO SVZ (Figure 3P). To further validate our observations, we performed immunofluorescence labeling with BrdU, TUJ1, and PDGFR. Using confocal microscopy and z-stack image analysis, we determined how many BrdU-positive cells were co-labeled with TUJ1 or with PDGFRα in each SVZ section. TUJ1 is abundantly expressed in the SVZ and striatum and this was apparent in both WT (Figure 3Q) and PARP-1 KO mice (Figure 3U). More BrdU-positive cells were apparent in PARP-1 KO mice (Figure 3V) than WT mice (Figure 3R). In agreement with our above observations, more PDGFRα-positive cells appeared in the SVZ of PARP-1 KO mice (Figure 3W) than WT mice (Figure 3S) and more of these cells appeared to co-label with BrdU in the PARP-1 KO SVZ (Figure 3X) than in the WT SVZ (Figure 3T). We counted the number of BrdU/TUJ1 and BrdU/PDGFRα double-labeled cells in the SVZ to solidify our observations. PARP-1 KO mice had significantly fewer BrdU/TUJ1 double-labeled neural progenitors in the SVZ than WT mice (Figure 3Y, $p<0.05$) and nearly three times as many BrdU/PDGFRα double-labeled cells as WT mice (Figure 3Z, $p<0.01$). Thus, PARP-1 KO mice display preference towards proliferating OPCs at the expense of proliferating neuroblasts. We also quantified PDGFRα cells in the SVZ and found a significant increase in PDGFRα cells in the SVZ of PARP-1 KO mice compared with WT mice (Figure 3AA, $p<0.01$), further documenting enhanced OPC presence in PARP-1 KO mice. In addition to these multi-label analyses, we examined BrdU and Olig2 immunofluorescence labeling to identify proliferating OPCs and lend further support to our hypothesis that PARP-1 KO mice display enhanced OPC production. We used confocal microscopy to quantify the number of BrdU-positive and BrdU/Olig2 double-positive cells. We observed increased BrdU/Olig2 expression in the SVZ of PARP-1 KO mice (Figure 3AC) compared with WT mice (Figure 3AB). We observed only about 9% of BrdU-positive cells in the SVZ co-expressing Olig2 in WT mice while 19% of BrdU-positive cells co-labeled with Olig2 in PARP-1 KO mice (Figure 3AD, $p<0.01$). Together, these data indicate that a fate switch occurs in the SVZ of PARP-1 KO mice, shifting neural stem cells from a neural progenitor to an OPC.

Decreased neuroblast presence without changes in SVZ size in PARP-1 KO mice

The postnatal SVZ contains type A, B, and C cells. Type B cells are the putative neural stem cells which can be identified by their GFAP expression and give rise to type C cells. Type C cells are the transit-amplifying cells which express the transcription factors DLX2 and Mash1. Type C cells give rise to type A cells, known as neuroblasts, and express DCX, polysialylated neural cell adhesion molecule, TUJ1 and Map2abc. In the adult brain, under physiological conditions, neuroblasts migrate out of the SVZ through the rostral migratory stream (RMS) and into the olfactory bulbs where they become interneurons. In the early postnatal brain, SVZ cells become astrocytes, oligodendrocytes or neurons and migrate into the nearby cortex, corpus callosum and striatum, in addition to the olfactory bulbs. Thus, postnatal SVZ neural stem cells give rise to neuroblasts as well as oligodendrocyte progenitors. As noted above, we found increased cell proliferation and a shift toward an oligodendroglial fate in the SVZ of PARP-1 KO mice. To further determine changes in the neuroblast population, we examined the area of DCX-positive cells in the SVZ, RMS, and olfactory bulb. Interestingly, we observed a decreased area of DCX-positive cells in the dorsolateral tail of the SVZ in PARP-1 KO mice (Figure 4B–C) compared to WT mice (Figure 4A, C, $p<0.05$). Similarly, the area of DCX-positive cells was also decreased in the RMS of PARP-1 KO mice (Figure 4E–F) compared with WT mice (Figure 4D, F, D, $p<0.05$). Despite these decreases, we observed no difference in the area of DCX-positive cells in the olfactory bulb subependymal layer of PARP-1 KO and WT mice (data not shown). Next we examined the total SVZ area using cresyl violet stained sections and the same quantification method with Image J. Interestingly, there was no difference in the total SVZ area, as displayed by cresyl violet staining, between PARP-1 KO (Figure 4H) and WT mice (Figure 4G, I), suggesting that the decreased DCX area did not lead to a smaller SVZ, rather that the SVZ cells were still present and likely acquired another fate.

PARP-1 deletion enhances oligodendrocyte progenitor production in the corpus callosum

Oligodendrocyte progenitor cells are present in the corpus callosum during the postnatal period and exist into adulthood. Due to their close proximity to the SVZ as well as the increased expression of OPC markers in the SVZ of PARP-1 KO mice, we examined whether the OPC population was also altered in the corpus callosum of these mice. We also examined the proliferating neuroblast population, as some neuroblasts are present in the corpus callosum. We first examined KI67/DCX expression in the corpus callosum and found no difference in the number of proliferating neuroblasts in the corpus callosum of PARP-1 KO and WT mice (Figure 5A). A small number of DCX-positive/KI67 negative cells were present in the corpus callosum of WT (Figure 5B, arrowheads) and PARP-1 KO (Figure 5C, arrowheads) mice as were a few DCX/KI67 double-labeled cells (Figure 5B–C, arrows). Next we examined proliferating OPCs using BrdU with PDGFRα or Olig2 antibodies. We counted the number of BrdU/PDGFRα double-labeled cells in the corpus callosum. We found a three-fold increase in the number of BrdU/PDGFRα double-labeled cells in the corpus callosum of PARP-1 KO mice (6.2 ± 1.8 cells/section) compared with WT mice (1.7 ± 0.4 cells/section, Figure 5D, $p<0.05$).This significant increase was apparent even without quantification (Figure 5E–F, arrows). To confirm increased presence of proliferating OPCs in the corpus callosum of PARP-1 KO mice, we also examined BrdU/Olig2 cells. We compared the total number of BrdU+ cells with the number of BrdU/Olig2 double-labeled cells to calculate the percentage of proliferating OPCs. More BrdU/Olig2 double-labeled cells appeared in the corpus callosum of PARP-1 KO mice than in WT mice (Figure 5H–I). Upon quantification, we discovered that approximately 30% of BrdU-positive cells co-expressed Olig2 in the corpus callosum of WT mice (Figure 5G), while 46% of BrdU cells co-labeled with Olig2 in PARP-1 KO mice (Figure 5G), representing a significant increase in these cells in PARP-1 KO mice ($p<0.01$). In addition, we examined the number of Olig1-positive OPCs present in the corpus callosum. We found a significant increase in Olig1-

positive cells in the corpus callosum of PARP-1 KO mice (Figure 5J, L, $p<0.05$) compared with WT mice (Figure 5J–K). In the adult brain, these cells appear to be a continuous presence generated in situ, rather than arising from the SVZ or another area and migrating to the corpus callosum. In these experiments we did not use cell tracking to confirm the origin of the BrdU/Olig2 or BrdU/PDGFRα double labeled cells in the corpus callosum. Thus, we do not know if these cells arose from the SVZ and migrated dorsally over this short distance or if these are proliferating in situ. Taken together, these results indicate that PARP-1 deletion enhances oligodendrocyte progenitor production in multiple areas of the brain.

Enhanced PARP-1 expression is found in neurogenic regions of wild-type mice, while alterations in postnatal neural stem cells lead to myelin deficiencies in PARP-1 KO mice

Previous work suggested that PARP-1 and Sox2 directly interacted in embryonic stem cells to regulate properties of these stem cells. Thus, we examined whether PARP-1 expression in WT mice corresponded with changes in Sox2 expression in the SVZ and whether this might be associated with OPCs. We performed triple label immunofluorescence for Sox2, PARP-1 and Olig2 expression in the SVZ of WT mice. Using confocal microscopy, we examined and counted double and triple labeled cells. PARP-1 was expressed at baseline levels in all cells and this was apparent in the WT mice (Figure 6A). Cells strongly expressing PARP-1 were rare (Figure 6A, arrowhead) in the SVZ. Olig2 (Figure 6B) and Sox2 expression were abundant in the SVZ of WT mice and occasionally co-localized (Figure 6D, arrows). As a positive control, tissue from a hypoxia-ischemia exposed WT mouse was stained and the presence of PARP-1 positive cells was more apparent, as some cells are activated as a result of injury and more strongly express PARP-1 (Figure 6E). Some of these activated PARP-1 cells also co-express Sox2 and Olig2 after hypoxia-ischemia (Figure 6E, arrowhead). To determine if PARP-1 and Sox2 expression coincided in OPCs, we examined the population of Olig2-positive cells and determined whether they also expressed PARP-1 or Sox2. The majority (54%) of Olig2-positive SVZ cells expressed Sox2 but not PARP-1 (Figure 6F) while 33% of Olig2-posive OPCs did not express Sox2 or PARP-1. Less than 10% of Olig2-positive cells expressed PARP-1 without Sox2 and only 5% expressed all three markers. Due to the difficulty in finding PARP-1 expressing cells in the SVZ, we also examined mRNA expression of these three markers. While this method does not give us information about co-localization, it does provide correlative data to further support our hypothesis that PARP-1 regulates SVZ neural stem cell fate. In addition, it lends support to the notion that PARP-1 expression may differ in the SVZ compared to other brain regions, thus providing influence on SVZ neural stem cells. We first examined PARP-1 mRNA expression in the SVZ of WT male and female mice in comparison to the non-neurogenic cortical region. We observed a significant increase in PARP-1 mRNA expression in the SVZ compared to the nonneurogenic brain region (Figure 6G, $p<0.05$). This suggests that deleting or inhibiting PARP-1 could alter the SVZ neural stem cells without affecting the entire brain, which expresses a lower baseline of PARP-1. Next, we examined Sox2 and Olig2 mRNA expression in the SVZ of PARP-1 KO and WT mice and compared this to the non-neurogenic control region. As expected, Sox2 mRNA was increased in the SVZ of WT mice compared to the non-neurogenic cortex (Figure 6H, $p<0.05$). Sox2 expression was increased nearly 6-fold in the SVZ of PARP-1 KO mice compared with the non-neurogenic cortex (Figure 6H, $p<0.01$) and was also significantly increased compared to the WT SVZ (Figure 6H, $p<0.05$). These data combined with our immunofluorescence results confirm that Sox2 expression is greatly enhanced in the SVZ of PARP-1 KO mice. We observed enhanced Sox2/Olig2 expression in the SVZ of PARP-1 KO mice and thus examined Olig2 mRNA expression as well. We found no difference in Olig2 mRNA expression between the non-neurogenic cortex and the WT SVZ (Figure 6I), however, Olig2 mRNA expression was significantly enhanced in the PARP-1 KO SVZ compared to the WT SVZ and to the non-neurogenic control region (Figure 6I, $p<0.01$).

We observed enhanced OPC presence in the SVZ and corpus callosum and enhanced BrdU/Olig2 in the corpus callosum of PARP-1 KO mice, and reasoned that the enhanced OPC proliferation could be due to alterations in myelination in the areas surrounding the SVZ. Myelinating oligodendrocytes begin to express myelin basic protein (MBP) when mice are approximately 11 days old. Thus, we examined the expression of MBP in the corpus callosum, overlying the SVZ, as well as the external capsule and striatum. We performed immunohistochemistry with an antibody for MBP and performed qualitative analysis on the corpus callosum and external capsule at the level of the striatum and SVZ. We observed a drastic thinning of the corpus callosum in PARP-1 KO males and females (Figure 6K, M), as shown by MBP expression, when compared to MBP expression in WT mice (Figure 6J, L). In addition to the band of myelination in the corpus callosum, MBP-positive cells extend dorsally into the cortex in WT mice (Figure 6J, L) and stretch midway through the cortex. In contrast, PARP-1 KO mice exhibit a much diminished extension of MBP-positive cells into the cortex (Figure 6K, M). Differences in MBP-positive immunoreactivity were also observed in the external capsule. Similar to the corpus callosum, MBP-positive cells appear less dense and do not extend out of the external capsule towards the cortex in PARP-1 KO mice (Figure 6O) to the extent of those cells in WT mice (Figure 6N). Clusters of MBP-positive cells are present in the striatum as well. It is difficult to determine whether differences in myelination occur in the striatum of PARP-1 KO mice, however, the clusters appear slightly smaller in PARP-1 KO mice (Figure 6Q) than in WT mice (Figure P). To further evaluate the effects of PARP-1 depletion on myelination, we performed immunofluorescence staining with antibodies for Sox10, an oligodendrocyte progenitor marker, and O4, a marker for immature myelinating oligodendrocytes. We observed enhanced Sox10 expression in PARP-1 KO mice (Figure 6S) compared with WT mice (Figure 6R). We also performed qPCR experiments to examine the expression of Sox10 from the P11 wildtype and PARP-1 KO samples. Our results indicated that there was an increase in the Sox10 level in PARP-1 KO mice by 38 ± 4.5% ($n = 8$, $p<0.05$) as compared to wildtype mice. These results suggest that PARP-1 depletion regulates oligodendrocyte progenitors in the corpus callosum, in addition to the SVZ. Analysis of the early myelination marker O4 revealed the opposite trend of that seen with Sox10, with decreased O4 expression in the corpus callosum of PARP-1 KO mice (Figure 6U) compared with WT mice (Figure 6T). This suggests that immature myelinating oligodendrocytes as well as mature myelinating oligodendrocytes, as seen with MBP, are deficient in PARP-1 KO mice. Taken together, these data indicate that SVZ neural stem cells promote OPC generation in an attempt to reconcile for decreased myelination in PARP-1 KO mice.

PARP-1 deficiency reduces size

A recent study identified a role for PARP-1 in regulating weight gain when they observed that adult PARP-1 KO mice on a high fat diet gained more weight than their wild-type counterparts (Devalaraja-Narashimha and Padanilam). They suggested that this increased weight gain was not due to increased consumption, but due to decreased metabolic rate and energy expenditure instead. This finding prompted us to examine the brain and body sizes of postnatal mice and to determine if intrinsic differences existed in these mice from an early age. Mice were sexed and litters of equal number were weighed on P11. We found significant differences in body weight at this young age. PARP-1 KO males weighed significantly less than WT males (Figure 7A, 6.37 ± 0.1 g vs. 6.74 ± 0.12 g, $p<0.05$) as did PARP-1 KO females (Figure 7A, 6.49 ± 0.08 g vs. 6.83 ± 0.14 g, $p<0.05$). Next, we sought to determine if brain size was also altered in PARP-1 KO mice. The same mice that were used for the body weight analysis were included in the brain weight analysis. Mice were anesthetized, decapitated and the entire brain removed, including the olfactory bulbs, forebrain, midbrain, hindbrain, and cerebellum and weighed. Interestingly, PARP-1 KO males and females had significantly smaller brain weights compared with their respective

WT counterparts (Figure 7B, KO-M: 0.35 ± 0.00 g vs. WT-M: 0.37 ± 0.00 g, KO-F: 0.32 ± 0.00 g vs. WT-F: 0.36 ± 0.00, $p<0.01$). Due to the smaller body and brain size, we next examined whether the smaller brain size was due to a smaller forebrain, where the SVZ is located, or due to differences in other areas of the brain. We performed cresyl violet staining to assess hemisphere area at the level of the forebrain SVZ. We found that hemisphere size at the level of the SVZ was also decreased in the forebrain of PARP-1 KO males and females compared with WT mice (Figure 7C, KO-M: 20.13 ± 0.24 mm^2 vs. WT-M: 21.88 ± 0.42 mm^2, KO-F: 20.00 ± 0.31 mm^2 vs. WT-F: 21.29 ± 0.52 mm^2, $p<0.05$). As shown above, we found no difference in the cresyl violet-positive SVZ area (Figure 5G–I). Thus, although the overall brain size decreased, SVZ size is unaffected by PARP-1 KO. We report myelin deficiencies accompanied by enhanced OPC production at the expense of neuroblast production in the PARP-1 KO mice, which may correspond to decreased brain size without decreased SVZ size. Thus, these data indicate that PARP-1 depletion alters brain size without altering the size of the neurogenic zone.

Discussion

PARP-1 is important in a number of cellular processes and is implicated in stem cell maintenance and differentiation. To date, no studies examined whether PARP-1 modulates postnatal neural stem cells. Here we thoroughly studied how PARP-1 deletion alters postnatal SVZ neural stem cells by examining proliferation and differentiation in PARP-1 KO mice compared with WT mice.

Due to a recent report suggesting an interaction between Sox2 and PARP-1 in regulating embryonic stem cells (Gao et al., 2009), we examined Sox2 expression levels in PARP-1 KO mice and discovered, similar to embryonic stem cells, that PARP-1 deletion enhances Sox2 expression in neural stem cells. Sox2 is a well-established stem cell factor so it is not surprising that its expression level is altered in the SVZ of postnatal PARP-1 KO mice. In the aforementioned embryonic stem cell study, PARP-1 inhibition compromised cell survival during the differentiation phase but not in undifferentiated embryonic stem cells. Thus, we examined whether the enhanced Sox2 population in PARP-1 KO mice contributed to altered neurogenesis or oligodendrogliogenesis, as both of these processes occur at this postnatal age. We discovered that Sox2 upregulation preferentially occurred in Olig2-positive OPCs in PARP-1 KO mice rather than in neuroblasts, which suggests that PARP-1 may play a role in regulating cell fate. It is plausible that PARP-1 depletion up-regulates Sox2 to enhance proliferation and promote glial fate while contributing to decreased neuroblast survival. A previous report suggested that PARP-1 directly poly(ADP-ribosyl)ates Sox2 to alter its downstream target gene, FGF4 (Gao et al., 2009). PARP-1 acts as a co-factor with Sox2 and Oct4 to regulate FGF4 expression during differentiation in ESCs. This interaction may persist in postnatal neural stem cells to maintain multipotency of SVZ neural stem cells. To solidify a fate switch in the SVZ neural stem cells of PARP-1 KO mice, we performed numerous sets of triple-labeling using BrdU or KI67 to assess proliferation combined with OPC markers (Olig1, NG2, PDGFR) and neuroblast markers (DCX, TUJ1). We found an upregulation of proliferating OPCs that occurred simultaneously with a downregulation of proliferating neuroblasts in the PARP-1 KO mice. In addition, we examined the OPC population alone and discovered an increase in their presence in the SVZ, regardless of whether they co-labeled with BrdU or KI67. Thus, these data suggest that PARP-1 deletion leads to a fate switch from neuroblast to OPC in the postnatal SVZ. As a final measure to solidify this conclusion, we examined BrdU and Olig2 double-labeled cells. A significantly greater percentage of BrdU cells co-labeled with Olig2 in the SVZ of PARP-1 KO mice than WT, further confirming an enhanced OPC presence. To date no studies have reported a role of PARP-1 in regulating neurogenesis. Our data provide novel evidence suggesting that PARP-1 functions to maintain neurogenesis in postnatal SVZ

neural stem cells, while its deletion promotes an oligodendroglial fate. PARP-1 acts as a co-factor in multiple biological pathways. It is likely that it regulates neurogenesis though interaction with transcription factors or downstream targets of Sox2, such as FGF4 and other pro-neural genes. It is likely that PARP-1 interactions that are not yet established could play a role in the balance amongst factors that control cell fate. There is a delicate balance between multiple factors controlling proliferation and differentiation in the SVZ. PARP-1 may regulate directly or indirectly factors such as the pro-neural gene EGF which promotes OPC fate, and that may tip the scales in favor of one phenotype over another (Gonzalez-Perez and Alvarez-Buylla). Mash1 is another pro-neural gene whose transcriptional mechanisms have been established in the postnatal SVZ (Parras et al., 2004). In addition, PARP-1 complexes with Mash1, Hes1, and TLE during *in vitro* differentiation of neural stem cells, which suggests that it could also play a role in postnatal SVZ neural stem cell differentiation (Ju et al., 2004).

We observed increased neural stem cell proliferation in the PARP-1 KO SVZ as measured by BrdU and KI67 labeling. This increase could be explained several ways. PARP-1 is a known regulator of chromatin structure. Its modification of chromatin structure is often determined by the amount of NAD+ present as well as autoPARylation of PARP-1 (Kim et al., 2005; Wacker et al., 2007). PARP-1 can promote chromatin compaction or disrupt chromatin structure by PARylating histones. In our study, lack of PARP-1 may facilitate chromatin relaxation, allowing for greater plasticity and SVZ proliferation. An alternative is that SVZ neural stem cell proliferation is enhanced because a greater percentage of cells are in the active stem cell state. The neural stem cell marker Sox2 was recently shown to act as a cofactor with PARP-1 to regulate mouse ESCs. PARP-1 inhibition increased the association of Sox2 with FGF4 enhancers in mouse ESCs and increased Sox2 protein expression (Gao et al., 2009). Our findings are similar, with significantly elevated levels of Sox2 protein expression in PARP-1 KO SVZ neural stem cells. Sox2 protein expression increased to a similar rate as proliferation in the PARP-1 KO SVZ. Thus, increased proliferation correlated with enhanced stem cell gene expression. This enhanced proliferation could lead to an overall increase in the neural stem cell population or may be due to enhanced proliferation of a specific cell type. We examined the percentage of BrdU cells expressing Olig2 and found this was enhanced in PARP-1 KO mice, suggesting that it is not simply a function of increased proliferation, but rather due to a change in SVZ neural stem cell fate. Of note, we found no obvious change in GFAP expression in the SVZ with immunofluorescence staining or mRNA expression between PARP-1 KO and WT mice (data not shown).

To further confirm decreased neurogenesis in the PARP-1 KO mice, we evaluated DCX staining using DAB as the chromogen to obtain a more sensitive reading of the neuroblast population. We performed area analyses on the SVZ, RMS, and olfactory bulb to identify whether the region of DCX-positive cells was altered in size. Interestingly we found a decrease in the DCX-positive area in the SVZ and RMS of PARP-1 KO mice but no changes in the olfactory bulb subependymal area. This may be due to in situ proliferation of neuroblasts in the olfactory bulb itself. In addition, factors regulating neuroblast presence could be altered. Notch activation increases SVZ cell proliferation and is expressed in DCX-positive cells (Wang et al., 2009); it also promotes proliferation and myelin formation in peripheral nervous tissue (Woodhoo et al., 2009). Decreased SVZ neuroblast presence could be due not only to altered regulation of neuroblast factors but also to differences in factors regulating glial fate.

Due to the enhanced presence of Olig2+/Sox2+ cells in the PARP-1 KO mice and the previously established relationship between PARP-1 and Sox2 in embryonic stem cells, we examined the expression pattern of PARP-1 in Olig2 and Sox2 cells in the SVZ of WT mice. PARP-1 is expressed at very low levels in nearly all cells at baseline and it was difficult to

distinguish its presence. We examined the Olig2 SVZ population to determine if PARP-1 displayed any preference towards these cells and if this had any correlation with Sox2. We found very few cells that more strongly expressed PARP-1 along with Sox2 and Olig2 or with either marker alone. Due to the difficulty in locating and analyzing the PARP-1 cell population in normal mice, we performed qPCR to more closely evaluate PARP-1 presence in the SVZ. With this method we found upregulated PARP-1 mRNA expression in the SVZ of WT mice compared to the non-neurogenic cortex. Enhanced PARP-1 expression in neurogenic versus non-neurogenic regions suggests that its deletion or inhibition could alter neurogenesis in regions where this process occurs. While it is impossible to determine co-localizations using qPCR, we also identified upregulated Sox2 expression in the WT SVZ compared to the non-neurogenic region and further upregulation in the PARP-1 KO SVZ compared to the WT SVZ. In addition, Olig2 mRNA expression was significantly increased in the PARP-1 KO mice compared to WT SVZ or the non-neurogenic cortex. Thus, these data confirm the correlation between Sox2 upregulation and PARP-1's role as a neurogenic niche modulator. In addition, our results also indicated that there was an approximately 38% increase in the level of the oligodendrocyte-specific Sox family factor Sox10 in PARP-1 KO mice as compared to wildtype mice, suggesting that PARP-1 regulates both Sox2 and Sox10, and that the regulation of Sox factors by PARP-1 could be a driver behind the SVZ phenotype in PARP-1 KO mice. Thus, PARP-1 may have a more broad effect on other Sox family members such as Sox10 that is a specific oligodendroglial lineage gene important for myelination, in addition to the PARP-1-mediated post-translational modification of Sox2, providing an additional interesting insight into oligodendrocyte biology.

Oligodendrocyte maturation starts to peak at P11 and the presence of OPCs remains high at this postnatal age in rodents. OPCs are located throughout the brain but are most concentrated in the corpus callosum, where myelination is prevalent. OPCs can be derived in situ but some may also migrate from the SVZ into the corpus callosum and other nearby regions during this postnatal period (Levison and Goldman, 1993). Since OPC proliferation/production is enhanced in the SVZ in PARP-1 KO mice, we examined oligodendrocyte proliferation in the corpus callosum to determine if changes also occurred in this area adjacent to the SVZ where the OPC population is prevalent. Interestingly, we found enhanced OPC production and OPC proliferation in the corpus callosum of PARP-1 KO mice. Olig2 is a pro-oligodendroglial gene and is up-regulated in PARP-1 KO mice, contributing to enhanced OPC presence in the SVZ and corpus callosum. This finding was confirmed using a panel of well-studied OPC markers, all of which were upregulated in PARP-1 KO mice. Finally, we examined whether myelination was altered in the corpus callosum and other areas near the SVZ to determine if enhanced OPC presence may be a result of altered myelination. Surprisingly, we found a severe reduction in myelination in the corpus callosum, external capsule, cortex, and to a lesser extent in the striatum in PARP-1 KO mice. We also noted decreased brain size in PARP-1 KO mice. Decreased myelination in these mice likely contributes to their smaller brain size as well as promotes OPC production. Together, these data indicate that hypomyelination occurs as a result of PARP-1 depletion, resulting in smaller brain size and more active SVZ neural stem cells which promote oligodendroglial fate to compensate for these deficiencies.

In summary, our findings identify a novel role for PARP-1 in regulating postnatal forebrain SVZ neural stem cells and provide yet another molecule involved in the complex stem cell regulatory network. While the SVZ phenotype in the PARP-1 mutant mice reveals an important function of PARP-1 in neural stem cell regulation, our results suggest that it is possible that PARP-1 has both direct and indirect effects on SVZ neural stem cell fates. The effects may result from a developmental adaptation of the brain in an attempt to compensate for the lack of myelination. Our results also demonstrate that PARP-1 deletion increases OPC proliferation. To compensate for deficiency in myelination in the corpus callosum, it is

possible that PARP-1 deficiency affects OPC migration. Overall, by carefully investigating the cellular composition of the SVZ and the neighboring white matter tract in PARP-1 knockout mice, the present study reveals previously unknown effects of PARP-1 deletion on mouse postnatal SVZ neural stem cells and the unexpected oligodendroglial fate and myelination. These findings prompt further exploration of PARP-1 inhibitors on SVZ neural stem cells and myelination. Currently PARP-1 inhibitors are viewed as a promising therapeutic agent for stroke and cancer. The evidence presented here suggests that these inhibitors may have unwanted side effects on neural stem cells. In addition, it appears that PARP-1 inhibitor treatment should be considered for demyelinating diseases, as it promotes OPC production in myelinating and neurogenic areas. Future studies should aim to examine the effects of PARP-1 depletion/inhibition on OPC maturation to determine if this poses a suitable treatment option. Finally, these studies examined the effects of PARP-1 deletion on postnatal SVZ neural stem cells. Further studies are needed to examine the effects on adult neural stem cells in the SVZ as well as those present in the dentate gyrus.

Acknowledgments

This work was supported by grants to W.D. from the NIH (RO1 NS059043 and RO1 ES015988), National Multiple Sclerosis Society, Feldstein Medical Foundation and Shriners Hospitals for Children. J.M.P was supported by a postdoctoral training grant from the NIEHS. The authors would like to thank Youning Zhang, Florian Mayrhofer, Olga Chechneva, and Daniel Daugherty for technical assistance.

References

Altman J. Autoradiographic and histological studies of postnatal neurogenesis. IV. Cell proliferation and migration in the anterior forebrain, with special reference to persisting neurogenesis in the olfactory bulb. J Comp Neurol. 1969; 137:433–457. [PubMed: 5361244]

Ame JC, Spenlehauer C, de Murcia G. The PARP superfamily. Bioessays. 2004; 26:882–893. [PubMed: 15273990]

Carlen M, Meletis K, Goritz C, Darsalia V, Evergren E, Tanigaki K, Amendola M, Barnabe-Heider F, Yeung MS, Naldini L, Honjo T, Kokaia Z, Shupliakov O, Cassidy RM, Lindvall O, Frisen J. Forebrain ependymal cells are Notch-dependent and generate neuroblasts and astrocytes after stroke. Nat Neurosci. 2009; 12:259–267. [PubMed: 19234458]

Chambon P, Weill JD, Mandel P. Nicotinamide mononucleotide activation of new DNA-dependent polyadenylic acid synthesizing nuclear enzyme. Biochem Biophys Res Commun. 1963; 11:39–43. [PubMed: 14019961]

Corotto FS, Henegar JA, Maruniak JA. Neurogenesis persists in the subependymal layer of the adult mouse brain. Neurosci Lett. 1993; 149:111–114. [PubMed: 8474679]

Coskun V, Wu H, Blanchi B, Tsao S, Kim K, Zhao J, Biancotti JC, Hutnick L, Krueger RC Jr. Fan G, de Vellis J, Sun YE. CD133+ neural stem cells in the ependyma of mammalian postnatal forebrain. Proc Natl Acad Sci U S A. 2008; 105:1026–1031. [PubMed: 18195354]

Devalaraja-Narashimha K, Padanilam BJ. PARP1 deficiency exacerbates diet-induced obesity in mice. J Endocrinol. 205:243–252. [PubMed: 20338998]

Doetsch F, Garcia-Verdugo JM, Alvarez-Buylla A. Cellular composition and three-dimensional organization of the subventricular germinal zone in the adult mammalian brain. J Neurosci. 1997; 17:5046–5061. [PubMed: 9185542]

Fernet M, Ponette V, Deniaud-Alexandre E, Menissier-De Murcia J, De Murcia G, Giocanti N, Megnin-Chanet F, Favaudon V. Poly(ADP-ribose) polymerase, a major determinant of early cell response to ionizing radiation. Int J Radiat Biol. 2000; 76:1621–1629. [PubMed: 11133044]

Fontan-Lozano A, Suarez-Pereira I, Horrillo A, del-Pozo-Martin Y, Hmadcha A, Carrion AM. Histone H1 poly[ADP]-ribosylation regulates the chromatin alterations required for learning consolidation. J Neurosci. 30:13305–13313. [PubMed: 20926656]

Gao F, Kwon SW, Zhao Y, Jin Y. PARP1 poly(ADP-ribosyl)ates Sox2 to control Sox2 protein levels and FGF4 expression during embryonic stem cell differentiation. J Biol Chem. 2009; 284:22263–22273. [PubMed: 19531481]

Goldberg S, Visochek L, Giladi E, Gozes I, Cohen-Armon M. PolyADP-ribosylation is required for long-term memory formation in mammals. J Neurochem. 2009; 111:72–79. [PubMed: 19645746]

Gonzalez-Perez O, Alvarez-Buylla A. Oligodendrogenesis in the subventricular zone and the role of epidermal growth factor. Brain Res Rev. 67:147–156. [PubMed: 21236296]

Hassa PO, Hottiger MO. The functional role of poly(ADP-ribose)polymerase 1 as novel coactivator of NF-kappaB in inflammatory disorders. Cell Mol Life Sci. 2002; 59:1534–1553. [PubMed: 12440774]

Hernandez AI, Wolk J, Hu JY, Liu J, Kurosu T, Schwartz JH, Schacher S. Poly-(ADP-ribose) polymerase-1 is necessary for long-term facilitation in Aplysia. J Neurosci. 2009; 29:9553–9562. [PubMed: 19641118]

Ju BG, Solum D, Song EJ, Lee KJ, Rose DW, Glass CK, Rosenfeld MG. Activating the PARP-1 sensor component of the groucho/ TLE1 corepressor complex mediates a CaMKinase IIdelta-dependent neurogenic gene activation pathway. Cell. 2004; 119:815–829. [PubMed: 15607978]

Kaplan MS, Hinds JW. Neurogenesis in the adult rat: electron microscopic analysis of light radioautographs. Science. 1977; 197:1092–1094. [PubMed: 887941]

Kim MY, Zhang T, Kraus WL. Poly(ADP-ribosyl)ation by PARP-1: `PAR-laying' NAD+ into a nuclear signal. Genes Dev. 2005; 19:1951–1967. [PubMed: 16140981]

Kraus WL, Lis JT. PARP goes transcription. Cell. 2003; 113:677–683. [PubMed: 12809599]

Krishnakumar R, Gamble MJ, Frizzell KM, Berrocal JG, Kininis M, Kraus WL. Reciprocal binding of PARP-1 and histone H1 at promoters specifies transcriptional outcomes. Science. 2008; 319:819–821. [PubMed: 18258916]

Krishnakumar R, Kraus WL. The PARP side of the nucleus: molecular actions, physiological outcomes, and clinical targets. Mol Cell. 39:8–24. [PubMed: 20603072]

Levison SW, Goldman JE. Both oligodendrocytes and astrocytes develop from progenitors in the subventricular zone of postnatal rat forebrain. Neuron. 1993; 10:201–212. [PubMed: 8439409]

Livak KJ, Schmittgen TD. Analysis of relative gene expression data using real-time quantitative PCR and the 2(-Delta Delta C(T)) Method. Methods. 2001; 25:402–408. [PubMed: 11846609]

Lois C, Alvarez-Buylla A. Proliferating subventricular zone cells in the adult mammalian forebrain can differentiate into neurons and glia. Proc Natl Acad Sci U S A. 1993; 90:2074–2077. [PubMed: 8446631]

Lois C, Alvarez-Buylla A. Long-distance neuronal migration in the adult mammalian brain. Science. 1994; 264:1145–1148. [PubMed: 8178174]

Masson M, Niedergang C, Schreiber V, Muller S, Menissier-de Murcia J, de Murcia G. XRCC1 is specifically associated with poly(ADP-ribose) polymerase and negatively regulates its activity following DNA damage. Mol Cell Biol. 1998; 18:3563–3571. [PubMed: 9584196]

Meyer-Ficca ML, Meyer RG, Jacobson EL, Jacobson MK. Poly(ADP-ribose) polymerases: managing genome stability. Int J Biochem Cell Biol. 2005; 37:920–926. [PubMed: 15743666]

Miller MW, Nowakowski RS. Use of bromodeoxyuridine-immunohistochemistry to examine the proliferation, migration and time of origin of cells in the central nervous system. Brain Res. 1988; 457:44–52. [PubMed: 3167568]

Moroni F. Poly(ADP-ribose)polymerase 1 (PARP-1) and postischemic brain damage. Curr Opin Pharmacol. 2008; 8:96–103. [PubMed: 18032109]

Nasta F, Laudisi F, Sambucci M, Rosado MM, Pioli C. Increased Foxp3+ regulatory T cells in poly(ADP-Ribose) polymerase-1 deficiency. J Immunol. 184:3470–3477. [PubMed: 20208002]

Ogino H, Nozaki T, Gunji A, Maeda M, Suzuki H, Ohta T, Murakami Y, Nakagama H, Sugimura T, Masutani M. Loss of Parp-1 affects gene expression profile in a genome-wide manner in ES cells and liver cells. BMC Genomics. 2007; 8:41. [PubMed: 17286852]

Parras CM, Galli R, Britz O, Soares S, Galichet C, Battiste J, Johnson JE, Nakafuku M, Vescovi A, Guillemot F. Mash1 specifies neurons and oligodendrocytes in the postnatal brain. EMBO J. 2004; 23:4495–4505. [PubMed: 15496983]

Plane JM, Liu R, Wang TW, Silverstein FS, Parent JM. Neonatal hypoxic-ischemic injury increases forebrain subventricular zone neurogenesis in the mouse. Neurobiol Dis. 2004; 16:585–595. [PubMed: 15262271]

Plane JM, Whitney JT, Schallert T, Parent JM. Retinoic acid and environmental enrichment alter subventricular zone and striatal neurogenesis after stroke. Exp Neurol. 2008; 214:125–134. [PubMed: 18778705]

Quenet D, El Ramy R, Schreiber V, Dantzer F. The role of poly(ADP-ribosyl)ation in epigenetic events. Int J Biochem Cell Biol. 2009; 41:60–65. [PubMed: 18775502]

Sodhi RK, Singh N, Jaggi AS. Poly(ADP-ribose) polymerase-1 (PARP-1) and its therapeutic implications. Vascul Pharmacol. 53:77–87. [PubMed: 20633699]

Sugimura K, Takebayashi S, Taguchi H, Takeda S, Okumura K. PARP-1 ensures regulation of replication fork progression by homologous recombination on damaged DNA. J Cell Biol. 2008; 183:1203–1212. [PubMed: 19103807]

Tartier L, Spenlehauer C, Newman HC, Folkard M, Prise KM, Michael BD, Menissier-de Murcia J, de Murcia G. Local DNA damage by proton microbeam irradiation induces poly(ADP-ribose) synthesis in mammalian cells. Mutagenesis. 2003; 18:411–416. [PubMed: 12960408]

Wacker DA, Ruhl DD, Balagamwala EH, Hope KM, Zhang T, Kraus WL. The DNA binding and catalytic domains of poly(ADP-ribose) polymerase 1 cooperate in the regulation of chromatin structure and transcription. Mol Cell Biol. 2007; 27:7475–7485. [PubMed: 17785446]

Wang X, Mao X, Xie L, Greenberg DA, Jin K. Involvement of Notch1 signaling in neurogenesis in the subventricular zone of normal and ischemic rat brain in vivo. J Cereb Blood Flow Metab. 2009; 29:1644–1654. [PubMed: 19536070]

West MJ, Ostergaard K, Andreassen OA, Finsen B. Estimation of the number of somatostatin neurons in the striatum: an in situ hybridization study using the optical fractionator method. J Comp Neurol. 1996; 370:11–22. [PubMed: 8797153]

Woodhoo A, Alonso MB, Droggiti A, Turmaine M, D'Antonio M, Parkinson DB, Wilton DK, Al-Shawi R, Simons P, Shen J, Guillemot F, Radtke F, Meijer D, Feltri ML, Wrabetz L, Mirsky R, Jessen KR. Notch controls embryonic Schwann cell differentiation, postnatal myelination and adult plasticity. Nat Neurosci. 2009; 12:839–847. [PubMed: 19525946]

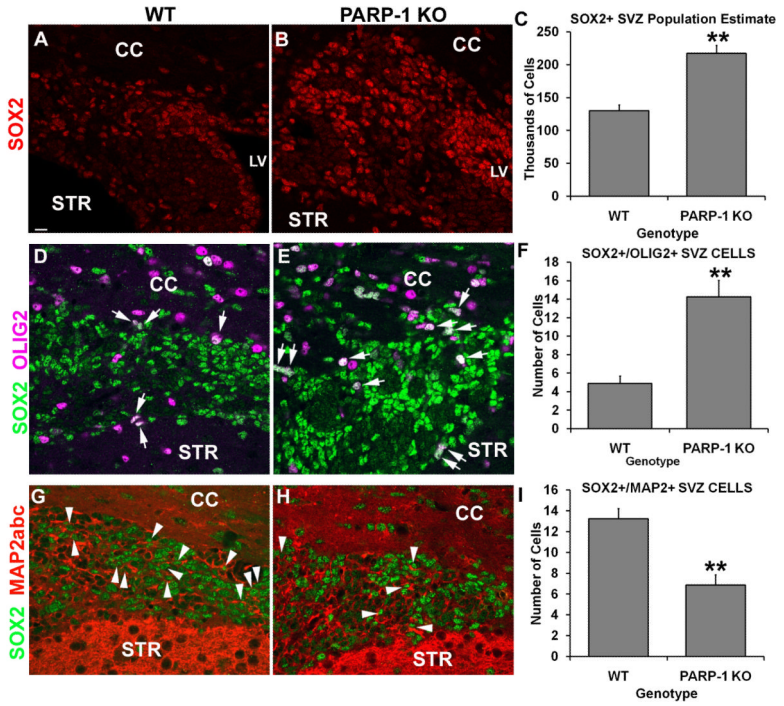

Figure 1. PARP-1 deletion enhances Sox2/Olig2+ precursor cells in the SVZ

Immunofluorescence labeling was performed to identify Sox2, Olig2, Map2abc and DAPI positive cells. PARP-1 KO mice (B) appear to have more Sox2-positive cells in the SVZ than their WT counterparts (A). To confirm this, we performed unbiased stereology on the SVZ to obtain a population estimate for this region. Stereological analyses confirmed that there was a significant increase in the number of Sox2-positive cells in the SVZ of PARP-1 KO mice compared with WT controls (C, **p<0.01). To confirm the progenitor fate of these cells, we performed immunofluorescence labeling for Sox2, Olig2, Map2abc and DAPI. Confocal microscope images were collected and analyzed to determine the number of Sox2+/Olig2+ or Sox2+/Map2abc+ double-labeled cells within the SVZ. We found more Sox2+/Olig2+ cells present in the SVZ of PARP-1 KO mice (E) than in WT mice (D). Quantification confirmed a significant increase in these cells in the PARP-1 KO mice compared with WT mice (F, **p<0.01). In addition, PARP-1 KO mice appeared to have fewer Sox2+/Map2abc+ double-labeled cells present in the SVZ (H) than their WT counterparts (G). These observations were confirmed with quantification (I, **p<0.01). All data are shown with SEM. Scale bar: 15 μm; CC: corpus callosum; LV: lateral ventricle; STR: striatum.

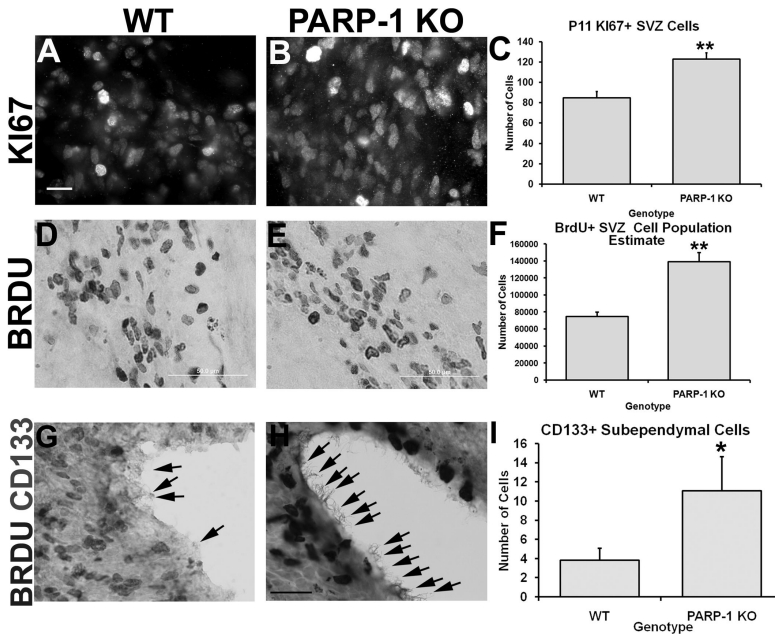

Figure 2. PARP-1 deletion enhances SVZ cell proliferation

(A–C) P11 mice were sacrificed to assess SVZ proliferation using immunofluorescence labeling for KI67. Four static images of the SVZ were collected and cells in the dorsolateral SVZ counted for each animal. PARP-1 KO mice had significantly more KI67+ cells (B, C, **p<0.01) than WT mice (A, C). (D–F) To confirm the effects on SVZ proliferation, mice were injected with BrdU (100 mg/kg, i.p.) 2 hours prior to sacrifice. Immunohistochemistry was performed to identify BrdU-positive cells in the SVZ and stereology performed to obtain a population estimate for the dorsolateral SVZ. PARP-1 KO mice (E) appeared to have significantly more BrdU-positive SVZ cells than WT mice (D), which was confirmed with stereology (F, **p<0.01). Coronal forebrain sections were immunostained with an antibody to CD-133 (prominin-1) to identify ependymal cells that may act as neural stem cells. Sections were double-stained with an antibody to BrdU to determine if CD133+ cells in the lateral ventricle are actively proliferating. Very few CD133+ cells were labeled along the lateral ventricle in P11 WT mice (G) and were generally found at the posterior striatal level, just before the appearance of the hippocampus. Numerous CD133+ cells were apparent in the PARP-1 KO ependymal layer (H). Quantification confirmed a significant increase in CD133+ cells in PARP-1 KO mice compared with WT mice (I, *p<0.05). All data are shown with SEM. Scale bars: 25 μm in A for A–B; 50 μm in D–E; 25 μm in H for G–H.

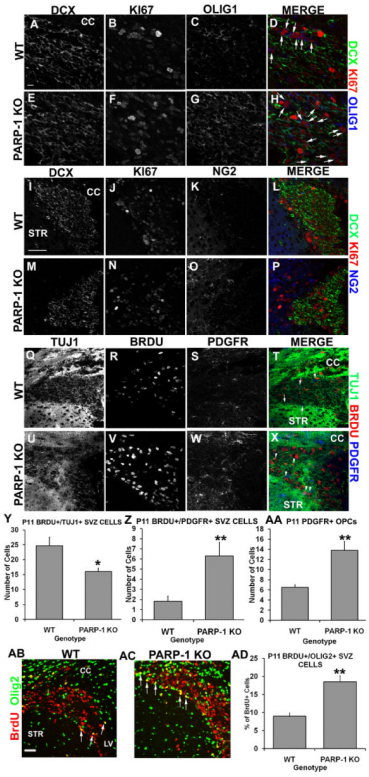

Figure 3. PARP-1 deletion shifts SVZ neural stem cells from neuronal to glial fate

Mice were injected with BrdU 2 hours prior to sacrifice. Immunofluorescence labeling was performed with Olig1, NG2 or PDGFR to identify OPCs, BrdU or KI67 to identify proliferating cells, and DCX or TUJ1 to identify neuroblasts. More KI67+/Olig1+ double-labeled cells appeared in the SVZ of PARP-1 KO mice (F, G, arrows in H) than in WT mice (B, C, arrows in D). Numerous DCX+ cells were present in WT (A) and PARP-1 KO (E) mice, however, more KI67+/DCX+ cells appeared in the WT SVZ (D) than in the PARP-1 KO SVZ (H). Triple label immunofluorescence with DCX/KI67/NG2 further revealed a greater presence of DCX+/KI67+ in WT mice (I, L) than in PARP-1 KO mice (M, P). We observed an increase in NG2+ cell presence in the SVZ of PARP-1 KO mice (O) along with an increased presence of NG2+/KI67+ SVZ cells (P) compared to WT mice (K, L). To further identify cell fate changes, we examined TUJ1/BrdU/PDGFR triple labeling in the SVZ. We observed a strong presence of TUJ1 in the WT (Q) and PARP-1 KO mouse (U), with many BrdU+/TUJ1+ cells also present in the WT (T) and PARP-1 KO (X) SVZ. More PDGFR+ cells appeared in the SVZ of PARP-1 KO mice (W) than in the WT (S, arrows in T) with an enhanced presence of BrdU+/PDGRF+ cells in the SVZ of PARP-1 KO mice (arrowheads in X) compared to WT mice (T). We quantified the number of BrdU+/TUJ1+ and BrdU+/PDGFR+ cells in the SVZ. We found significantly fewer BrdU+/TUJ1+ cells in the SVZ of PARP-1 KO mice compared with WT mice (Y, *$p<0.05$). In addition, we found significantly more BrdU+/PDGFR+ cells in the SVZ of PARP-1 KO mice than WT mice (Z, **$p<0.01$). We quantified PDGFR1+ cells in the SVZ to see if the total number of OPCs varied between WT and KO and we found significantly more PDGFR1+ cells in the SVZ of PARP-1 KO mice than in WT mice (AA, **$p<0.01$) We also performed immunofluorescence staining with antibodies to BrdU and Olig2 to identify and further quantify proliferating OPCs in the SVZ. The number of BrdU+ and BrdU+/Olig2+ cells was quantified using confocal microscopy. PARP-1 KO mice (AC) appear to have more BrdU+/Olig2+ cells (arrows) present in the SVZ than their WT counterparts (AB). Quantification revealed that PARP-1 KO mice have almost twice as many BrdU+/Olig2+ cells in the SVZ

as their WT counterparts (AD, **p<0.01). Scale bars: 10 μm in A for A–H; 50 μm in I for I–X; 25 μm in AB for AB–AC; CC: corpus callosum; STR: striatum; LV: lateral ventricle.

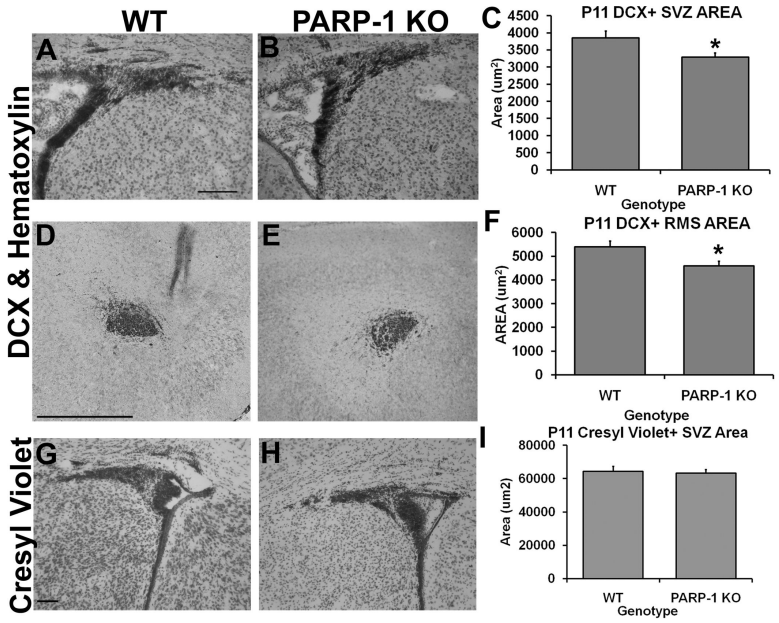

Figure 4. PARP-1 deletion decreases the presence of DCX+ SVZ and RMS area without altering overall SVZ size

Sections were immunostained with an antibody to DCX to identify the neuroblasts (type A cells) in the SVZ and RMS. The DCX+ area of the dorsolateral SVZ and RMS was obtained using Image J software. We found decreased DCX+ SVZ area in PARP-1 KO mice (B, C, *$p<0.05$) and this was significantly reduced compared to WT mice (A). We also observed a decrease in the area of DCX+ cells in the RMS of PARP-1 KO mice (E) compared with WT mice (D), which was significant upon quantification with Image J (F, *$p<0.05$). There was no difference in the total SVZ area as measured with Image J on cresyl violet stained sections in WT (G) or PARP-1 KO mice (H–I). All data are shown with SEM. Scale bars: 125 μm in A for A–B; 500 μm in D for D–E; 100 μm in G for G–H.

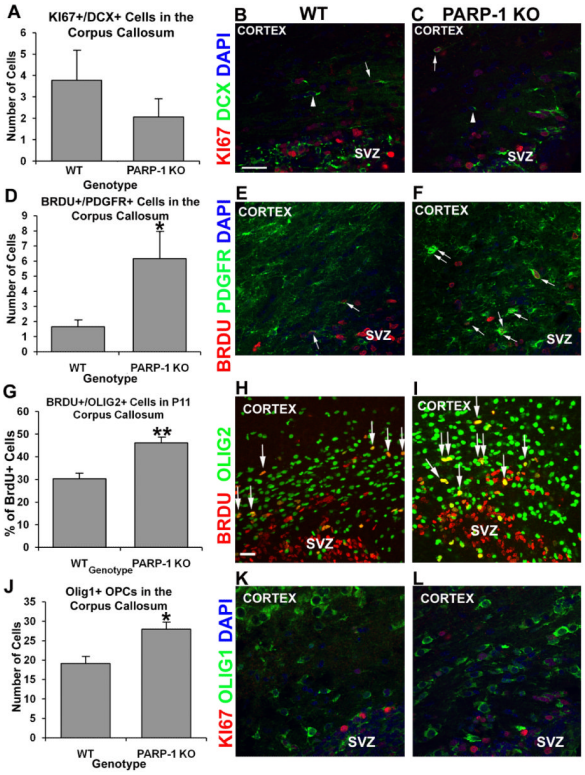

Figure 5. Loss of PARP-1 enhances oligodendrocyte progenitor production in the corpus callosum

Mice were injected with BrdU 2 hours prior to sacrifice. We performed immunofluorescence staining with antibodies to BrdU or KI67 and PDGFR, Olig1, and Olig2 to identify proliferating OPCS and with DCX to identify neuroblasts. We found no difference in the number of KI67+/DCX+ neuroblasts in the corpus callosum (A) between P11 WT (A, arrow in B) and PARP-1 KO mice (A, arrow in C). The number of BrdU+/PDGFR+ cells significantly increased in the corpus callosum of PARP-1 KO mice (D, *p<0.05, arrows in F) compared with WT mice (D, arrows in E). To confirm increased OPC proliferation, we counted BrdU+/Olig2+ cells in the corpus callosum. We observed a significantly greater percentage of BrdU+ cells co-expressing Olig2 in the corpus callosum of PARP-1 KO mice (G, **p<0.01, arrows in I) than in WT mice (G, arrows in H). In addition, we counted the number of Olig1+ cells present in the corpus callosum. We found significantly more Olig1+ OPCs in the corpus callosum of PARP-1 KO mice (J, *p<0.05, L) than in WT mice (J–K). Some Olig1+ cells co-labeled with KI67, both in WT mice (K) and PARP-1 KO mice (L). All data are shown with SEM. Scale bars: 25 μm in B for B–F, K–L; 25 μm in H for H–I; SVZ: subventricular zone.

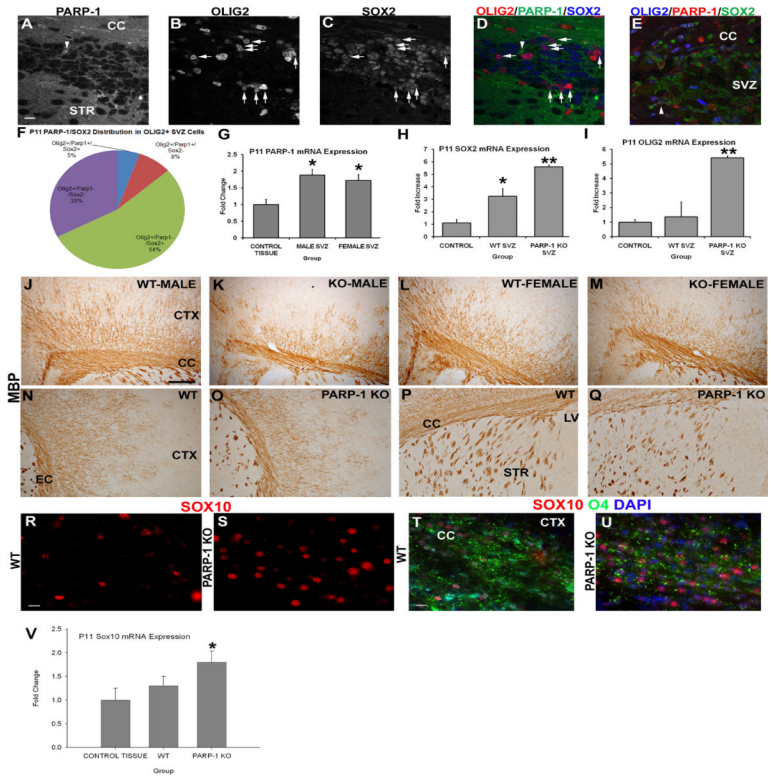

Figure 6. PARP-1 deletion upregulates expression of Sox2 and Sox10 and enhances the OPC population to compensate for the deficiency in myelination

(A–E) Immunofluorescence labeling was performed on WT mice to identify Sox2, Olig2 and PARP-1 positive cells. PARP-1 is expressed at low levels throughout the brain, making it difficult to identify positive cells. In WT mice, very few SVZ cells expressed PARP-1 above baseline levels (A). These cells rarely expressed Olig2 (B) or Sox2 (C). Numerous Sox2+ cells (blue in D) are present in the SVZ (C) and many co-localize with Olig2 (red; arrows in D) but not PARP-1 (green in D). As a positive control for the PARP-1 antibody, the same immunofluorescence staining was performed on a SVZ section from a mouse exposed to hypoxia-ischemia, and upregulated PARP-1 expression is seen in the SVZ, as shown by an Olig2+/Sox2+/PARP-1+ cell (arrowhead in E). Close examination of the Olig2+ population in the SVZ of WT mice using confocal microscopy revealed that 54% of Olig2+ cells also express Sox2 but not PARP-1 while 33% of Olig2+ cells do not express either marker (F). On average, 8% of Olig2+ cells expressed PARP-1 in the SVZ while only 5% expressed all 3 markers (F). We examined mRNA expression in the SVZ to determine if PARP-1 was elevated in the WT mice. PARP-1 mRNA expression significantly increase in the SVZ of WT male and female mice compared to the nonneurogenic control tissue (G, *$p<0.05$). Sox2 mRNA expression increased in the SVZ of PARP-1 KO mice nearly 6-fold compared to the non-neurogenic control region and was significantly elevated compared to WT mice (H, **$p<0.01$). Olig2 mRNA expression was also increased nearly 6-fold in the SVZ of PARP-1 KO mice compared to the non-neurogenic control tissue (I). Olig2 mRNA expression was significantly elevated in the SVZ of PARP-1 knockout mice compared to the SVZ of WT mice (I, **$p<0.01$). (J–Q) Due to differences in oligodendrocyte progenitor numbers, we examined whether mature oligodendrocytes were affected in the PARP-1 KO mice. We performed immunohistochemistry with an antibody to myelin basic protein (MBP) to identify mature, myelinating oligodendrocytes. Examination of the corpus callosum overlying the SVZ revealed a decrease in the thickness of this area in PARP-1 KO mice (K, M) compared with WT mice (J, L). In addition to the thinner band of MBP-positive cells

within the corpus callosum, fewer MBP+ cells appear to branch dorsally from the corpus callosum into the cortex and their location appears to be more restricted as well in PARP-1 KO mice (K, M) compared to WT mice (J, L). Examination of the external capsule revealed a similar reduction in MBP expression in PARP-1 KO mice (O) compared to WT mice (N), with KO mice displaying less dense MBP+ expression in the cortical region located lateral to the external capsule. Differences in MBP expression were less obvious in the striatum of PARP-1 KO mice (Q) compared with WT mice (P) but may be prevalent in this region as well. (R–U) We performed immunofluorescence to identify Sox10-positive and O4-positive oligodendroglial cells in the corpus callosum. We found enhanced Sox10 expression in the corpus callosum of PARP-1 KO mice (S) compared with WT mice (R). In addition, Sox10 mRNA expression measured by qPCR significantly increased in the PARP-1 KO as compared to WT mice (V, *$p<0.05$). Using O4 immunofluorescence staining, we noted decreased myelination in the corpus callosum of PARP-1 KO mice (U) compared with their WT counterparts (T). All data are shown with SEM. Scale bars: 10 μm in A (for A–E); 250 μm in J for J–P; 25 μm in R for R–S; 25 μm in T for T–U; CC: corpus callosum; STR: striatum; SVZ: subventricular zone; LV: lateral ventricle; CTX: cortex.

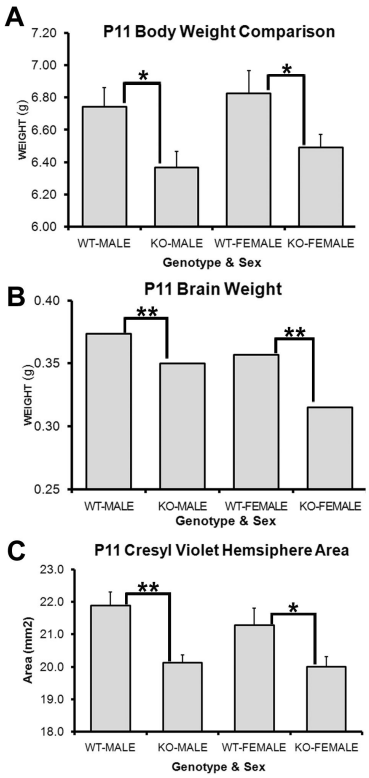

Figure 7. PARP-1 deletion decreases postnatal brain and body size

Mice were weighed at P11 and then sacrificed for wet brain weight. (A) Both male and female PARP-1 KO mice weighed significantly less than their WT counterparts (*$p<0.05$). (B) The entire brain was removed and weighed immediately after sacrifice. PARP-1 KOs had significantly smaller brains than male and female WT mice (**$p<0.01$). To confirm that this change was a result of differences in forebrain size, rather than cerebellar or hind-brain changes, brains were sectioned and stained for cresyl violet. Hemisphere areas were measured on 4 sections per animal at the level of the SVZ. (C) PARP-1 KO mice had significantly smaller forebrain hemispheres than WT mice, with slightly larger difference between males ($p<0.01$) than females ($p<0.05$). All data are shown with SEM.